SIMULATION OF AN ABSORPTION HEAT PUMP SOLAR HEATING AND COOLING SYSTEM

M. O. McLINDEN and S. A. KLEIN

Solar Energy Laboratory, University of Wisconsin–Madison, Madison, WI 53706, U.S.A.

Abstract—An absorption heat pump (AHP) is a heat driven heat pump utilizing the absorption process. A continuous, liquid absorbent AHP with chemical storage is modeled using mass and energy balances and assuming mass transfer equilibrium. This model is used with the TRNSYS program[5] to simulate the performance of an AHP in a residential solar-driven heating and cooling system. The effects of collector area for an AHP using the NaSCN–NH$_3$ chemical system are investigated for the Columbia, MO, Madison, WI, and Fort Worth, TX climates. The AHP system is compared to a conventional solar heating and cooling system and the effects of heat exchanger effectiveness, storage mass, additional thermal capacitance and alternative control strategies are studied for the Columbia climate.

INTRODUCTION

The absorption heat pump (AHP), through reversible absorption processes, uses the thermodynamic availability of a high temperature heat input to extract heat from a low temperature source and upgrade its temperature. An AHP is thus a type of heat-driven heat pump and uses the same basic cycle as an absorption air conditioner. The performance of a heat pump is measured in terms of its coefficient of performance (COP), defined as the ratio of the heating (or cooling) supplied by the heat pump to the high temperature heat input.

Energy storage in an AHP is achieved by separately storing the reacting chemicals[1]. This storage can be provided by inserting two storage tanks into the cycle: an absorbent tank between the generator and absorber and a refrigerant storage tank between the condenser and evaporator[2]. It is also possible to integrate the storage tanks with the reaction vessels (a combined condenser/refrigerant storage tank, for example). Since energy is stored in the form of chemical reaction potential, the reaction products can be stored at ambient temperatures; however, the sensible heat involved in cooling the products from the reaction temperature to ambient is lost. The addition of chemical energy storage to the cycle also allows the charging and discharging processes to be decoupled; for example, to provide cooling, only the evaporator and absorber need operate.

The characteristics of the absorption heat pump make it an interesting prospect for use in a solar heating and cooling system. The absorption cycle can pump heat across a useful temperature difference (e.g. from ambient to a 20°C heating load) with relatively low (*ca* 100°C) charging temperatures. Since the heating COP is greater than unity, it might be possible to use smaller collector areas as compared with a conventional liquid-based solar heating system having sensible heat storage. Auxiliary energy could be supplied through the AHP, taking advantage of its COP in the backup heating mode. This same AHP could also provide air conditioning and energy storage capabilities, eliminating the need for separate devices.

But these advantages do not come without penalties. A heating COP greater than one requires higher collector temperatures than a conventional solar heating system. The equipment that comprises a AHP is more complex than a conventional system (but perhaps comparable to a solar heating system combined with a solar-driven absorption air conditioner). Finally, chemical energy storage requires the containment of sizeable quantities of chemicals which may be expensive or hazardous.

The purpose of this paper is to investigate, through simulations, the thermal performance of absorption heat pumps in space conditioning applications. The systems to be considered are solar-driven; i.e. solar provides the high temperature energy required to drive the cycle. This is in contrast to other solar-assisted heat pump systems using vapor compression heat pumps where solar provides the low temperature energy to the evaporator[3].

SYSTEM DESCRIPTION

The absorption heat pump modeled is a continuous, liquid absorbent system with a combined condenser/refrigerant storage tank and an absorber/absorbent tank as shown in Fig. 1. This configuration is simpler than a system with separate storage tanks. It also has the ability to store thermal as well as chemical energy within the cycle by raising the temperature of the tank contents. This feature would allow, for example, the heat of condensation generated during the charging process to be stored if it were not immediately needed to meet the heating load. In air conditioning, a portion of the heats of absorption and condensation could be stored during the day and rejected at night, reducing the ambient heat exchanger requirements.

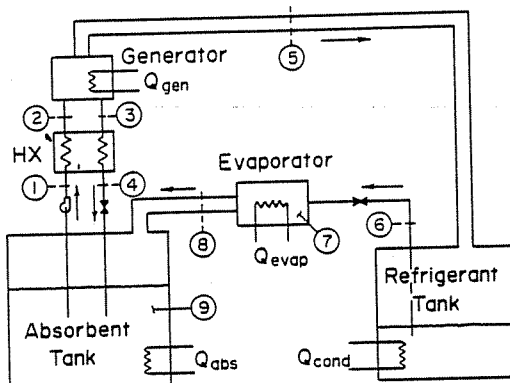This configuration has possible disadvantages.

Fig. 1. AHP configuration.

Storing the heat of condensation by raising the refrigerant tank temperature increases the temperature of the generator and that of the collector, thereby reducing collector efficiency. Offenhartz[4] has pointed out that thermodynamic availability may be lost by absorbing refrigerant directly in the absorbent tank rather than in a separate absorber where concentration can be controlled.

The complete heating and cooling system consists of the AHP, load, solar collector, ambient heat exchanger, etc. as shown in Fig. 2. This system was modeled with the simulation program TRNSYS[5]. This program links subroutines which model individual components of a complete system and solves the resulting system of algebraic and differential equations.

SYSTEM MODEL

The AHP model is based on mass and energy balances written around various parts of the cycle; it thus represents a thermodynamic approach rather than a "black box" approach using empirical performance curves. Correlations of thermodynamic and physical property data are supplied via subroutines, making the model independent of the chemical system. The major assumptions employed are that:

1. The reaction rates are controlled by heat transfer resistances, i.e. mass transfer equilibrium is achieved.
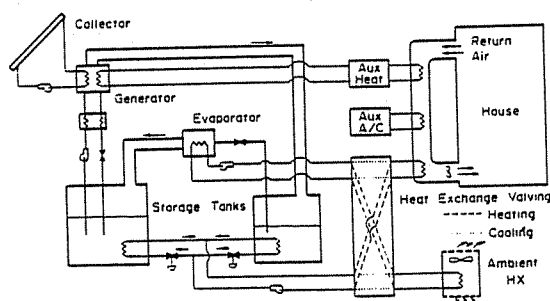
2. The thermal and mass capacitance of the generator and evaporator are negligible compared to those of the storage tanks.

3. All vessels are fully mixed.

4. The absorbent is completely non-volatile.

Thus, this model represents a limiting best case analysis in several respects.

Overall mass and energy balances are written for each tank and reaction vessel; absorbent mass balances are also written for the generator and absorbent tank. (In the following equations, numbered subscripts refer to points in Fig. 1. The sign convention employed is that heat flows into the system are positive and mass flows are positive in the direction of the arrows in Fig. 1.) For the generator plus heat exchanger these balances yield:

$$0 = \dot{m}_1 - \dot{m}_4 - \dot{m}_5 \tag{1}$$

$$0 = x_1 \dot{m}_1 - x_4 \dot{m}_4 \tag{2}$$

$$0 = \dot{m}_1 h_1 - \dot{m}_4 h_4 - \dot{m}_5 h_5 + \dot{Q}_{gen} + \dot{Q}_{aux} + \dot{Q}_{loss,g}. \tag{3}$$

For the refrigerant tank, the mass and energy balances give:

$$\frac{dm_c}{dt} = \dot{m}_5 - \dot{m}_6 \tag{4}$$

$$\frac{dU_c}{dt} = \dot{m}_5 h_5 - \dot{m}_6 h_6 + \dot{Q}_{cond} + \dot{Q}_{loss,c} \tag{5}$$

where $\dot{m}$ is mass flow rate, x is the mass fraction of absorbent, U is total internal energy and the $\dot{Q}$ terms are heat flows described below.

The assumption of mass transfer equilibrium implies:

$$P_1 = P_2 = P_3 = P_4 = P_5 = P_6. \tag{6}$$

This high side pressure relates the temperature and concentration in the generator with the refrigerant tank temperature; by choosing two, the third is determined. This relationship is shown in Fig. 3 where vapor pressure data for NaSCN–NH$_3$ have been plotted as vapor saturation (condenser) tem-

Fig. 2. Absorption heat pump solar heating and cooling system.
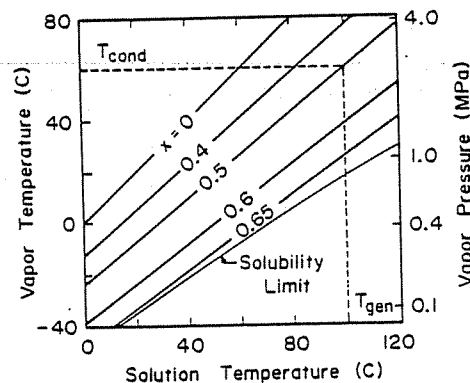
Fig. 3. Relationship between condenser temperature and generator concentration and temperature for NaSCN–NH$_3$.

perature vs liquid solution (generator) temperature. Note that the generator temperature is increased by an increase in concentration or condenser temperature.

Energy and mass balances on the counter-current heat exchanger (neglecting losses to the surroundings) yield:

$$\dot{m}_4 h_4 = \dot{m}_3 h_3 - \epsilon_{g-a}(\dot{m}C)_{min}(T_3 - T_1) \qquad (7)$$

$$\dot{m}_3 = \dot{m}_4 \qquad (8)$$

where ϵ_{g-a} is the effectiveness of the heat exchanger and $(\dot{m}C)_{min}$ is the minimum capacitance rate through the heat exchanger.

The $\dot{Q}_{aux}$ term in (3) is the rate of auxiliary heat input to the generator. The remaining heat flows in (3) and (5) are given by simple heat transfer relations. Modeling the heat exchangers in the tanks as constant effectiveness devices yields:

$$\dot{Q}_{gen} = (\dot{m}C)_{hx.g}\epsilon_g(T_{hx.g} - T_3) \qquad (9)$$

$$\dot{Q}_{cond} = (\dot{m}C)_{hx.c}\epsilon_c(T_{hx.c} - T_6) \qquad (10)$$

where $T_{hx.g}$ and $T_{hx.c}$ are the temperatures of the heat exchange streams entering the generator and refrigerant tank. The tank losses (actually negative heat gains because of the sign convention) are:

$$\dot{Q}_{loss.g} = UA_g(T_{env} - T_3) \qquad (11)$$

$$\dot{Q}_{loss.c} = UA_c(T_{env} - T_6) \qquad (12)$$

where T_{env} is the temperature of the tank environment.

A similar set of mass and energy balances can be written for the absorbent tank:

$$\frac{dm_a}{dt} = \dot{m}_4 + \dot{m}_8 - \dot{m}_1 \qquad (13)$$

$$\frac{dm_{abs.a}}{dt} = x_4\dot{m}_4 - x_1\dot{m}_1 \qquad (14)$$

$$\frac{dU_a}{dt} = \dot{m}_4 h_4 + \dot{m}_8 h_8 - \dot{m}_1 h_1 + \dot{Q}_{abs} + \dot{Q}_{loss.a} \qquad (15)$$

and evaporator:

$$0 = \dot{m}_6 - \dot{m}_8 \qquad (16)$$

$$0 = \dot{m}_6 h_6 - \dot{m}_8 h_8 + \dot{Q}_{evap} + \dot{Q}_{loss.e}. \qquad (17)$$

The heat flows in (15) and (17) are described by expressions analogous to (9)–(12). The assumption of mass transfer equilibrium implies:

$$P_7 = P_8 = P_9. \qquad (18)$$

In solving the above equations, the mass and internal energy derivatives are integrated by TRNSYS and supplied to the AHP component. The conditions in the tanks are then computed in terms of

the current values of U, m and m_{abs} using property subroutines discussed in the next section.

Property relations

The AHP model requires thermodynamic and physical property data for the chemical system used; in the TRNSYS model, curve fits to equilibrium property data are supplied via FORTRAN function subroutines. The two most important relations are the vapor pressure and enthalpy for a refrigerant–absorbent mixture as a function of temperature and concentration. Figure 3 shows vapor pressure data for the NaSCN–NH₃ chemical system. Routines are also needed which given the enthalpy and specific volume of refrigerant vapor as a function of temperature and pressure; the specific volume of the liquid as a function of temperature and concentration; and the temperature of a liquid mixture given either its enthalpy and concentration or its vapor pressure and concentration.

Also needed is an auxiliary subroutine, called TMIXU, which calculates the temperature and concentration of a two phase, two component mixture (with one component assumed non-volatile) in a tank. The inputs to TMIXU are the total internal energy and volume of the tank and the total mass of each component. This subroutine finds the temperature and liquid phase composition that satisfy the equations:

$$\frac{U_{tot}}{m_{tot}} = f u_{liq}(T, x) + (1 - f)u_{vap}(T, P)$$

$$+ \left[\frac{(mC)_{tank}}{m_{tot}}\right](T - T_{reference}) \qquad (19)$$

$$\frac{V_{tot}}{m_{tot}} = f v_{liq}(T, x) + (1 - f)v_{vap}(T, P) \qquad (20)$$

where U and V are total internal energy and volume in the tank, u and v are specific internal energy and volume and the subscripts tot, liq and vap refer to the total contents of the tank and the liquid and vapor phases respectively. The parameter f is the mass fraction of the tank contents in the liquid phase and $(mC)_{tank}$ represents the thermal capacitance of the tank, excluding the refrigerant and absorbent it contains. The concentration in the liquid phase is given by:

$$x = \frac{m_{abs}}{(m_{ref} + m_{abs})f} \qquad (21)$$

where m_{ref} and m_{abs} are the total masses of refrigerant and absorbent in the tank. The pressure P is a function of T and x. thus, (19) and (20) are functions of only T and f, and can be solved iteratively.

Load model

The heating and cooling load modeled in this study represents a two-story house with 165 m² of floor area. It utilizes a transfer-function load model and

temperature-level control as described in [5]. The infiltration rate is 0.5 air changes per hour and the walls and ceiling are insulated with 7.5 and 22.5 cm of fiberglass insulation, respectively. The overall loss coefficient is 167 W/°C. Internal heat generation averaged 656 W. Solar heat gains through windows are included but latent loads and domestic hot water loads are not.

Baseline control strategy

An absorption heat pump system has a large number of control options which may have a significant effect on its performance. Several strategies have been investigated. The baseline control strategy is determined, in large part, by a multi-stage room thermostat with the heating/cooling mode determined by the time of year. In the heating mode, as the room temperature falls, heat is supplied to the load first from the refrigerant tank and then from both tanks, provided that the tank temperatures are above some minimum useful temperature. (This order minimizes the generator, and thus collector, temperature.) As the room temperature falls below the third and fourth set points, auxiliary heat is added to the generator and then directly to the load.

All of these stages employ deadbands and can operate simultaneously except that auxiliary heat cannot be supplied both to the generator and directly to the load at the same time. The heating set points used in the simulations were 21, 20, 19 and 18°C with a 0.5°C deadband.

Cooling is supplied by the AHP when the room temperature rises above 23°C and the evaporator temperature is below a maximum value. Auxiliary cooling is provided by a separate vapor compression device and is supplied directly to the load when the room temperature exceeds 25°C. The ambient heat exchanger is modeled as a "dry" constant effectiveness device and operates when there is a minimum 2°C temp. difference between the ambient and evaporator temperatures in the heating season, or between the condenser or absorber temperature and ambient in cooling operation.

The collector is controlled in the conventional manner with a differential on–off controller sensing the collector and generator temperatures. The collector and auxiliary input to the generator are not operated when the system is fully charged (to prevent crystallization of absorbent out of solution at high concentration).

Alternate control strategies

In addition to the baseline control strategy presented above, two other heating season control strategies were considered. In order to study the interaction between solar and auxiliary energy supplied through the generator, the auxiliary mode was disabled. Supplying auxiliary through the heat pump takes advantage of its greater than one COP but it results in a higher average state of charge of the

system which leads to higher collector temperatures and reduced energy storage capacity for solar energy.

During times of marginal solar collection, the greater than one COP gained by supplying solar through the heat pump may be more than offset by low collection efficiency. During these times, the overall system performance might be improved if solar energy could "bypass" the generator and deliver heat at a lower temperature. In the second alternate control strategy, collected energy is delivered to the absorbent storage tank rather than to the generator when:

$$\frac{\eta_{bypass}}{COP\eta_{gen}} > 1 \qquad (22)$$

where η_{bypass} and η_{gen} are the collection efficiencies when delivering heat to the absorbent tank and generator. This option was implemented by computing each efficiency using the Hottel–Whillier[6] collector equation and using an average COP. Although it would be difficult to physically construct, this method of implementation serves to identify the value of this control option.

Chemical system

The chemical system chosen for use in this study employs ammonia (NH_3) as the refrigerant and a solution of sodium thiocyanate (NaSCN) and ammonia as the absorbent. This choice is based primarily on two considerations. The low freezing point of ammonia allows wintertime heat pumping and thermodynamic data are available for this refrigerant–absorbent pair[7, 8]. It is recognized that this system may not be optimum from thermodynamic, safety and practical standpoints. For example, there is disagreement in the literature regarding the corrosiveness of NaSCN[7–9].

The effects of different chemical systems are considered by simulating an AHP using sulfuric acid and water. The data given in [10, 11] were used to generate the necessary property correlations. The vapor pressure of water was extrapolated below the freezing point to allow wintertime heat pumping. It is possible to use water below 0°C by adding an anti-freeze to the evaporator although this would lower the vapor pressure and reduce the temperature difference across which heat could be pumped.

Storage capacity of an AHP

The storage capacity of an AHP is the useful energy obtainable as the system goes from fully charged to fully discharged. Using the NaSCN–NH$_3$ chemical system, the maximum mass fraction of absorbent is about 0.65 due to the crystallization limit. The minimum useful mass fraction is about 0.50, corresponding to a heat pumping temperature difference of 30°C. Thus, if there are equal masses of absorbent and refrigerant in the cycle (to give $x = 0.50$ when fully discharged), the amount of "active" refrigerant, i.e. the amount that must be boiled

off to yield a concentration of 0.65, is 46 per cent of the refrigerant or 23 per cent of the total system mass.

In a fully charged system, 77 per cent of the system mass is in the absorbent tank with $x = 0.65$. During discharging, the other 23 per cent of the mass enters the absorbent tank as refrigerant vapor, yielding a final state with all of the mass in the absorbent tank. Assuming equal initial and final temperatures the internal energy change in this process is 410 kJ kg^{-1}. Add to this the thermal storage capacity of the chemicals over a 30°C temperature swing to yield a total energy storage capacity of roughly 500 kJ kg^{-1}. By comparison, a water tank with a 60°C temperature swing stores about 250 kJ kg^{-1}.

The cooling energy storage capacity would approximately be the fraction of "active" refrigerant multiplied by its heat of vaporization or about 290 kJ kg^{-1}. Stored thermal energy is not directly usable during the cooling season but, as will be seen, may have other performance benefits. Unpressurized hot water storage for a conventional absorption chiller would have a useful temperature swing of about 20°C; taking into account a COP of 0.7 for the chiller, the cooling storage capacity would be 50 kJ kg^{-1}. The energy storage capacities for the sulfuric acid–water chemical system are 1150 kJ kg^{-1} for heating and 870 kJ kg^{-1} for cooling.

Conventional solar heating/cooling system

For comparison, a liquid-based solar heating system with sensible heat storage was simulated. It includes a solar-fired lithium bromide–water absorption chiller with an evaporative cooling tower. This system was modeled with standard TRNSYS components and, except for using the transfer function load model as described above, is very similar to the example solar heating and cooling system given in the TRNSYS manual[5].

RESULTS AND DISCUSSION

Heating season and cooling season simulations were conducted with the absorption heat pump model to determine the effects of several design variables and control options. The primary index of system performance is F_{NP}, the fraction of the total load met by nonpurchased energy, defined as:

$$F_{NP} = 1 - \frac{Q_{aux}}{Q_{load}} \qquad (23)$$

where Q_{aux} is the total auxiliary supplied and Q_{load} is the total energy used to meet the heating or cooling load. The important fixed parameters used in the simulation are as listed in Table 1 (except where noted in the text). The collector is modeled as a flat plate, but the values of $F_R U_L$ and $F_R(\tau\alpha)$ were chosen to represent an evacuated tubular collector.

Effects of collector area and storage mass

The AHP system was simulated using SOLMET TMY weather data[12] for Columbia, MO with

Table 1. Fixed simulation parameters

Collector	
slope = latitude	
$\dot{m}_{col}/A_{col}$	0.015 kg sec^{-1} m^{-2}
$F_R(\tau\alpha)$	0.55
$F_R U_L$	0.833 W m^{-2} c^{-1}
Heat exchangers	
ε_{g-a}	0.75
ε (all other heat exchangers)	0.60
heat transfer fluid capacitance	3.5 kJ kg^{-1} c^{-1}
Heat exchanger flow rates	
$\dot{m}_{g-a}$	150 kg hr^{-1}
$\dot{m}_{abs} + \dot{m}_{cond}$	1500 kg hr^{-1}
$\dot{m}_{evap}$	1500 kg hr^{-1}
$\dot{m}_{ambient}$ (air side)	2500 kg hr^{-1}
$\dot{m}_{load}$ (air side)	2500 kg hr^{-1}
Storage Tanks	
height/diameter ratio	1.0
loss coefficient	0.437 W m^{-2} c^{-1}

three collector areas and two storage sizes (expressed as total mass of refrigerant and absorbent) to determine the effect of these variables on system performance and to identify appropriate base case values for subsequent comparisons. The timestep for most of the simulations was 0.2 hr. The results presented in Fig. 4 show that the AHP supplies a significant fraction of the heating load with nonpurchased energy at zero collector area. This is because the auxiliary energy input through the heat pump can extract additional energy from ambient and deliver it to the load. In the cooling season, the F_{NP} curve starts at zero because here the useful energy flow is the low temperature heat extracted from the load. The cooling results for 1000 and 2000 kg of storage were virtually identical, indicating that a "plateau" may have been reached in the F_{NP} vs storage curve. For heating, the two storage size curves intersect; at low
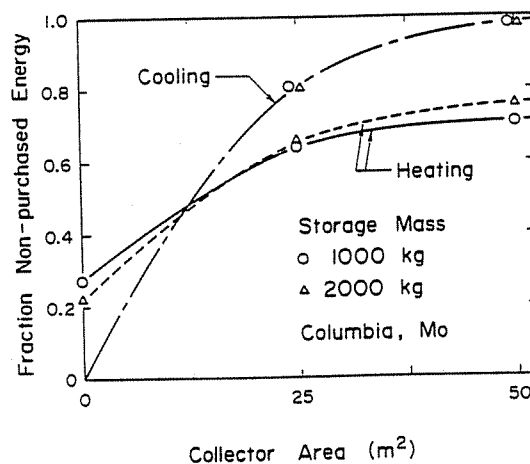

Fig. 4. Effect of collector area and storage mass on seasonal F_{NP} for AHP system in Columbia.

collector areas, increased tank losses offset any effect of greater storage 'mass.

Monthly and seasonal average values of several quantities for the system with 1000 kg storage and 25 m² collector are shown in Table 2. The average collector operating temperature is quite high (137°C in January and 115°C in July). It is higher in January than July because of the higher condenser temperature and higher absorbent concentration. This is primarily because auxiliary energy input through the generator keeps the system at a moderately high state of charge during mid-winter. This, combined with lower ambient temperatures, results in a January collector efficiency that is substantially lower than the July figure and roughly half of its maximum value (i.e. $F_R(\tau\alpha)$). The January heating COP is 1.403 and the July cooling COP is 0.546. The heating COP is penalized because of tank losses.

Table 2. Average collector and refrigerant tank temperature, absorbent tank concentration, collector efficiency, COP, tank losses and load for base case simulation (Columbia, 1000 kg chemical storage, 25 m² collector)

	T_{col} (C)	T_{cond} (C)	x_{abs}	η_{col}	COP	q_{loss} (GJ)	q_{load} (GJ)
January	137.2	38.6	0.585	0.278	1.403	0.41	3.54
Heating Season (Oct-Apr)	151.1	49.2	0.610	0.204	1.334	4.18	36.49
July	115.4	32.8	0.524	0.423	0.546	0.31	6.09
Cooling Season (May-Sept)	117.1	28.2	0.548	0.392	0.522	1.22	19.80

Simulations were also carried out in the Columbia climate with the conventional solar heating and cooling system. The results of these simulations are given in Fig. 5. The conventional system, of course, provides no non-purchased energy with zero collector area. The F_{NP} curve however, has a much greater slope in the heating season than the AHP system because of lower average collector temperatures. Thus, the performance of the two systems approach each other at high collector areas. In the cooling season, the performance of the two systems is qualitatively similar; the LiBr–H₂O absorption chiller

provides a higher F_{NP} because of a combination of higher COP, lower collector temperatures and the lower cooling water temperatures provided by the evaporative cooling tower.

Effects of climate

The AHP system with 1000 kg of chemical storage was also simulated in the Madison and Fort Worth climates. The solar contribution to F_{NP} in the Madison heating season is relatively small as shown in Fig. 6. This is due to a combination of lower ambient temperatures and radiation levels as compared with Columbia, leading to low collector efficiency. During the cooling season, however, 25 m² of collector meets 92 per cent of the relatively small (12 GJ) load.

The opposite situation occurs in the Fort Worth climate. Here, 25 m² of collector can supply 84 per cent of the 13 GJ heating load with non-purchased energy as shown in Fig. 7. With 25 m² of collector, most of the auxiliary energy is required during a relatively few cold, cloudy days when the collector can not operate; thus an additional 25 m² of collector results in only a small increase in F_{NP}. The large (34 GJ) cooling load in Fort Worth, however, leads to the lowest cooling F_{NP} of the three locations.
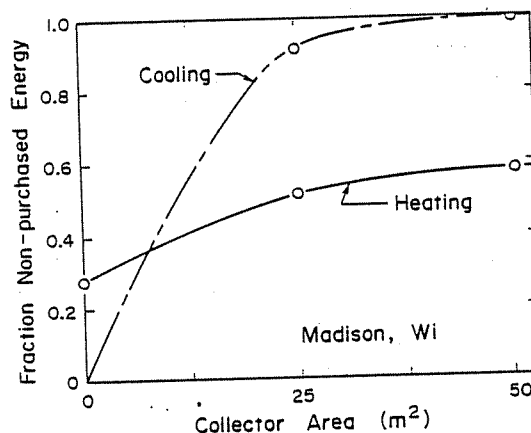
Fig. 6. Effect of collector area on seasonal F_{NP} for AHP system in Madison.
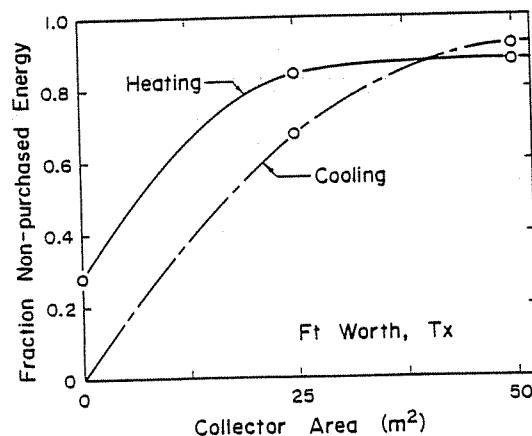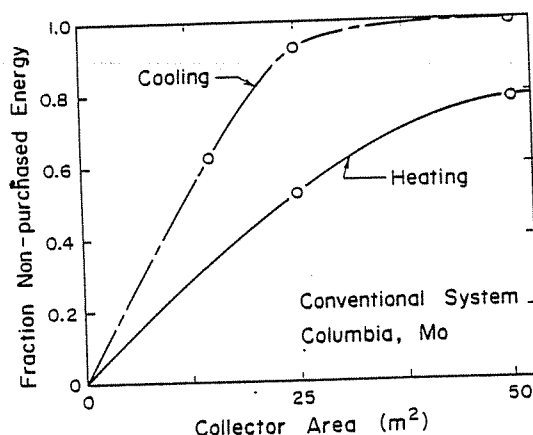
In order to evaluate the relative merits of the AHP system in the three locations, it is necessary to compare the magnitudes of the non-purchased energy provided by the system rather than the fraction of the total load. These results are given in Table 3. (The loads vary with collector area because systems which meet a higher fraction of the load keep the room temperature higher in the winter and lower in the summer). The total amount of non-purchased energy provided over the entire year is surprisingly similar between the three locations except for the zero collector area case. The incremental gain in total non-purchased energy in doubling the collector area from 25 m² to 50 m² is small. These figures would increase slightly if storage capacity were increased with collector area as shown in Fig. 4.

Table 3. Effect of location and collector area on fraction non-purchased energy, load and non-purchased energy delivered to load for systems with 1000 kg chemical storage

Col. Area (m²)	Heating			Cooling			Annual
	F_{NP}	Q_{load} (GJ)	Q_{NP} (GJ)	F_{NP}	Q_{load} (GJ)	Q_{NP} (GJ)	Q_{NP} (GJ)
Madison							
0	0.279	55.5	15.5	0	–	0	15.5
25	0.515	57.0	29.4	0.920	11.3	10.4	39.8
50	0.578	57.4	33.2	0.994	12.3	12.2	45.4
Columbia							
0	0.274	34.6	9.5	0	–	0	9.5
25	0.640	36.5	23.4	0.809	19.8	16.0	39.3
50	0.704	36.8	25.9	0.982	21.5	21.1	47.0
Fort Worth							
0	0.281	11.9	3.3	0	–	0	3.3
25	0.844	13.6	11.5	0.677	33.6	22.7	34.2
50	0.876	13.8	12.1	0.919	35.9	33.0	45.1

Effects of chemical system

The effects of the refrigerant–absorbent pair on performance were investigated by simulating an AHP using the sulfuric acid-water chemical system, but otherwise having the base case parameters. The seasonal values of collector efficiency and COP for the sulfuric acid system (given in Table 4) are slightly higher than those for the NaSCN system (given in Table 2). The sulfuric acid system provides a significantly higher value of F_{NP}. This result contradicts the speculation by Offenhartz[2] that the performance of all liquid absorbent chemical systems are similar; his conclusion was based on a limited comparison of the H_2SO_4–H_2O and NH_4NO_3–NH_3 systems.

The better performance of the sulfuric acid AHP is at least partially due to its higher equilibrium, steady state COP[13]. It also has a higher energy storage density and can pump heat across a slightly greater

Table 4. Average collector temperature and efficiency, COP and fraction non-purchased energy for sulfuric acid-water AHP with 25 m² collector and 1000 kg chemical storage

	T_{col} (C)	$\bar{\eta}_{col}$	COP	F_{NP}
January	122.6	0.315	1.447	0.609
Heating Season	162.9	0.240	1.365	0.734
July	100.0	0.418	0.661	0.661
Cooling Season	110.6	0.395	0.590	0.889

temperature difference than the NaSCN–NH₃ system for a given charging temperature. (For example, a generator temperature of 80°C and a condenser temperature of 40°C would yield an equilibrium mass fraction in the generator of 0.520 in the NaSCN system and 0.632 in the H_2SO_4 system; with these mass fractions in an absorber at 40°C, the equilibrium evaporator temperatures would be 6.8 and 4.8°C for the NaSCN and H_2SO_4 systems, respectively.)

Effects of heat exchanger effectiveness

The sensitivity of performance to the effectiveness of the heat exchangers in the system was studied. The results are given in Table 5. The effectiveness of the counter-current heat exchanger between the generator and absorbent tank, ϵ_{g-a}, was varied independently of all the others in the system, ϵ. Heating season performance is not very sensitive to varying ϵ_{g-a} but cooling season performance is quite markedly affected. With a lower ϵ_{g-a} a greater fraction of the energy input to the generator is required merely to raise the temperature of the incoming stream to the generator temperature, leaving less energy to boil off refrigerant. (This effect is reflected in the ratio of Q_{cond}/Q_{abs}.) This is not a severe penalty in heating since this energy can be recovered in the absorbent tank, although at a COP of essentially unity. Cooling, however, can be produced only by the evaporation of refrigerant; thus anything which reduces the vapor production rate in the generator will affect performance.

Table 5. Effect of heat exchanger effectiveness on F_{NP} and the ratio of the heats of condensation and absorption (seasonal results)

ϵ	ϵ_{g-a}	F_{NP}		Q_{cond}/Q_{abs}	
		heat	cool	heat	cool
0.60*	0.75*	0.640	0.809	0.752	0.705
0.30	0.75	0.496	0.707	0.729	0.674
0.30	0.35	0.470	0.497	0.392	0.388

*base case conditions

Effects of storage mass and additional thermal capacitance

The absorption heat pump configuration studied has the ability to store thermal energy. The above discussion of storage capacity, however, has shown the thermal storage capacity of the chemicals in the AHP to be relatively small. Thus in order to amplify any benefits of thermal storage, the effects of additional thermal capacitance were investigated. This additional capacitance was modeled as a separate water tank surrounding, and having the same temperature as, the refrigerant or absorbent tank.

The effects of thermal capacitance were simulated using August weather data with systems having 100 or 500 kg of chemical storage and 5000 kJ °C⁻¹ of thermal storage (corresponding to roughly 1200 l. of water) added either to the refrigerant tank or absorbent tank or split between the two. The results given

in Table 6 show a moderate increase in the fraction of non-purchased energy supplied to the load with either increased chemical storage or thermal capacitance.

Table 6. Effect of chemical storage mass and additional thermal capacitance on F_{NP} (August results)

Added thermal capacitance (kJ C^{-1})		F_{NP}	
ref tank	abs tank	m=100 kg	m=500 kg
0	0	0.634	0.711
2500	2500	0.682	0.746
5000	0	0.692	0.758
0	5000	0.668	0.726

Figure 8 shows the monthly average distribution of rejected heat (the sum of Q_{cond} and Q_{abs}) over the day for the cases of no additional capacitance and 2500 kJ/kg added to each tank for each of the two storage masses. The system with 100 kg of chemical storage and no additional thermal capacitance is typically fully discharged at 8.00 p.m. and cannot operate again until solar is input the next morning. With additional chemical storage the system does not swing from fully discharged to fully charged back to discharged in the course of a day. Additional thermal capacitance and, to a lesser extent, greater chemical storage mass result in a more nearly even rejection of heat over the entire day.

The combination of the larger storage mass and added thermal capacitance lowers the peak heat rejection rate from 33 to 19 MJ hr^{-1} and shifts it to later in the day. This ability to level out the heat rejected to ambient would permit the use of a smaller ambient heat exchanger or might permit the use of a "dry" heat exchanger rather than an evaporative cooling tower. These results are not very sensitive to where the additional capacitance is placed; splitting it between the condenser and absorber appears to offer a compromise between highest F_{NP} and lowest peak heat rejection rate.

January results for a system with 500 kg of chemical storage and varying thermal storage are given in
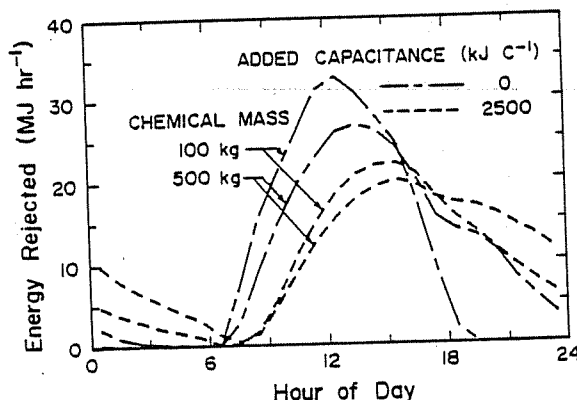

Fig. 8. Monthly average diurnal distribution of heat rejected to ambient during August for varying chemical

Table 7 and Fig. 9. In heating operation, additional thermal capacitance in the absorbent tank lowers its temperature and results in greater heat extraction from ambient during daytime hours. The resulting lower daytime absorbent concentration leads to lower collector temperatures and a higher value of F_{NP}. There is less heat extracted from ambient during the night because of lower average absorbent concentrations as compared with the case of no added thermal capacitance. Adding capacitance to the refrigerant tank has much less effect; there is little energy to store because the heat of condensation usually goes directly to the load. Increased tank losses (because of the larger tank surface area) decrease the value of F_{NP} for the case of 5000 kJ °C^{-1} added to the refrigerant tank.

Table 7. Effect of additional thermal capacitance on F_{NP}, absorbent tank concentration and collector energy for system in Columbia (January results; chemical storage mass = 500 kg)

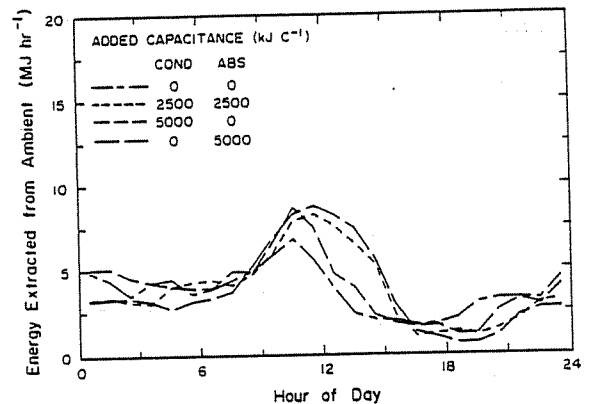| Added thermal capacitance (kJ C^{-1})		F_{NP}	x_{abs}	Q_{col} (GJ)
ref tank	abs tank			
0	0	0.478	0.595	1.97
2500	2500	0.491	0.589	2.12
5000	0	0.463	0.599	1.84
0	5000	0.501	0.580	2.17

Fig. 9. Monthly average diurnal distribution of heat extracted from ambient during January for varying thermal capacitance added to storage tanks; chemical mass = 500 kg.

Effects of alternate control strategies

The effects of the two alternate heating season control options described earlier were investigated. The simulations were performed with 25 m^2 of collector and 1000 kg of chemical storage and are compared to the base case results. Adding auxiliary energy through the heat pump takes advantage of its COP, but penalizes solar energy collection by raising the average absorbent concentration. This interaction is most pronounced when auxiliary input is high (i.e. mid-winter) and unimportant when solar is meeting a high fraction of the load as shown in Table 8. In April, solar supplies a high fraction of the load and

Table 8. Effect of not supplying auxiliary energy through the heat pump on absorbent tank concentration, collector temperature, collected and auxiliary energy and F_{NP} for system in Columbia

A-Auxiliary through heat pump (base case)

	x_{abs}	T_{col} (C)	Q_{col} (GJ)	Q_{aux} (GJ)	F_{NP}
January	0.585	137.3	2.27	3.93	0.540
April	0.637	168.3	1.64	0.08	0.953
Heating Season	0.610	151.1	14.65	12.88	0.640

B-No auxiliary input through heat pump

	x_{abs}	T_{col} (C)	Q_{col} (GJ)	Q_{aux} (GJ)	F_{NP}
January	0.558	120.8	2.80	4.49	0.452
April	0.636	169.4	1.71	0.11	0.938
Heating Season	0.595	141.4	16.31	15.04	0.573

the small quantity of auxiliary has little effect. In January, however, the alternate strategy of not supplying auxiliary through the generator significantly decreases the average absorbent concentration, resulting in lower collector temperatures, thus increasing the amount of solar energy collected. The overall performance, expressed by F_{NP}, is reduced when auxiliary is not supplied through the generator; the gain in collector performance is more than offset by not taking advantage of the COP of the heat pump in the back-up heating mode. This result applies to every month and the heating season as a whole.

The benefit of a greater than one heating COP comes at the expense of higher collector temperatures and thus overall performance might be improved if solar energy could "bypass" the generator and supply energy to the lower temperature absorbent tank. This control option should be more important as the collector loss coefficient increases. A collector with a $F_R U_L$ of 3.3 W m^{-2} °C^{-1} and a $F_R(\tau\alpha)$ of 0.70 (representing a single-glazed, selective surface, flat plate collector) was simulated in addition to the base case collector. Table 9 gives the results of these simulations.

For the high performance collector, the option of bypassing the generator resulted in a significantly larger total of collected energy as well as increased collector operating time. The value of F_{NP} is only slightly increased because much of the solar bypassing the generator is collected early and late in the heating season. During these times, the system is

Table 9. Effect of generator bypass control option and collector type on F_{NP}, collected energy and collector operating time for AHP system

A-Evacuated tubular collector (seasonal results)

Bypass	F_{NP}	Q_{col} (GJ)				col. on time (hrs)			
		gen	abs	tank	total	gen	abs	tank	total
no*	0.640	14.65	0		14.65	698	0		698
yes	0.672	10.67	11.29		21.96	480	654		1134

B-Evacuated tubular collector (January results)

| no* | 0.540 | 2.27 | 0 | | 2.27 | 112 | 0 | | 112 |
| yes | 0.578 | 2.35 | 0.52 | | 2.88 | 104 | 52 | | 156 |

C-Flat plate collector (seasonal results)

| no | 0.470 | 7.65 | 0 | | 7.65 | 400 | 0 | | 400 |
| yes | 0.564 | 3.56 | 12.07 | | 15.63 | 174 | 523 | | 697 |

*base case conditions

often fully charged and the collector is prevented from supplying energy to the generator. But it can (and does) supply energy to the absorbent tank where much of the additional collected energy is dissipated as increased tank losses. For this reason, the January results given in Table 9 are much more indicative of the actual merits of this strategy. These indicate that with high performance collectors there is a modest increase in F_{NP} as a result of this alternate control strategy.

The flat plate collectors provided significantly less solar energy and gave a lower value of F_{NP} than the evacuated tubular collector. With the option of bypassing the generator, the collected energy and F_{NP} increased significantly. In this case, however, only about 23 per cent of the solar was input through the generator of the AHP. These results strongly suggest that a solar-driven absorption heat pump requires high performance collectors (such as evacuated tubes) for effective operation.

CONCLUSIONS

A model of an absorption heat pump which is based on mass and energy balances written around the components has been developed for use with TRNSYS. Simulations using this model have shown that a solar-driven AHP system can supply a significant fraction of a residential heating and cooling load with non-purchased energy. The annual non-purchased energy supplied to the load was similar for the three locations studied. In the Columbia climate, the AHP system gave a higher F_{NP} than a conventional solar heating system at small collector areas, while with larger areas, the F_{NP} of the two systems approached each other. In the cooling season, the AHP system gave a lower F_{NP} than a solar-fired lithium-bromide absorption chiller with hot water storage.

The collector temperatures are high and thus high performance collectors (such as evacuated tubes) are required for effective solar operation. The performance of the AHP is affected by the effectiveness of the heat exchangers in the system; the heat exchanger between the generator and absorbent tank has a large effect in cooling operation. The refrigerant–absorbent pair has a significant effect on system performance, with the H_2SO_4–H_2O system having better performance than the NaSCN–NH$_3$ pair.

The two alternative heating season control strategies investigated have little advantage in the Columbia climate. Not supplying auxiliary energy through the heat pump increases solar energy collection at the expense of overall system performance. The option of "bypassing" the generator significantly improved performance only for the high loss collector studied.

Adding thermal capacitance and (to a lesser extent) additional chemical storage mass to the cycle has the effect of leveling out the daily profile of heat rejected to ambient during cooling operation. In the heating mode, additional thermal capacitance shifts the times of heat extraction from ambient more towards day-

time hours. In most cases, additional thermal capacitance resulted in a higher value of F_{NP}.

NOMENCLATURE

C	heat capacity
f	mass fraction in liquid phase of two phase mixture
F_{NP}	fraction non-purchased energy supplied to load
F_R	collector heat removal factor
h	specific enthalpy
m	tank or system mass
$\dot{m}$	mass flow rate
$(\dot{m}C)_{min}$	minimum capacitance rate through a heat exchanger
P	pressure
Q	integrated heat flow
$\dot{Q}$	heat flow rate
T	temperature
u	specific internal energy
U	total internal energy
UA	loss coefficient-area product
U_L	collector loss coefficient
v	specific volume
V	volume (of tank)
x	mass fraction of absorbent
ϵ	heat exchanger effectiveness
η	collector efficiency
$(\tau\alpha)$	collector transmittance-absorptance product

Subscripts

a	absorber/absorbent tank
abs	absorbent species or absorption
aux	auxiliary energy
bypass	energy bypassing generator
c	condenser/refrigerant tank
col	collector
cond	condensation
e	evaporator
env	tank environment
evap	evaporation
g	generator
$g-a$	countercurrent heat exchanger between generator and absorber
hx	heat exchange stream
load	heating or cooling load
NP	non-purchased energy

ref	refrigerant species
tank	absorbent or refrigerant tank (non including contents)
tot	total contents of tank
1–9	system locations defined by Fig. 1

REFERENCES

1. P. O'D. Offenhartz, Chemical methods of storing solar energy. *Joint Conf. Am. Can. Sec. ISES* **8**, 48, Winnipeg (1976).
2. P. O'D. Offenhartz, TRNSYS simulation of chemical heat pumps for solar heating, cooling and storage. *Systems Simulation and Economic Analysis Conf.*, San Diego (1980).
3. T. L. Freeman, J. W. Mitchell and T. E. Audit, Performance of combined solar-heat pump systems. *Solar Energy* **22**, 125 (1979).
4. P. O'D. Offenhartz, Thermal storage studies for solar heating and cooling: applications using chemical heat pumps. *Final Report for DOE Contract* DE-AC02-79CS30428 (1980).
5. S. A. Klein *et al.*, *TRNSYS—A Transient Simulation Program.* University of Wisconsin-Madison, Engineering Experiment Station Report 38.11 (1981).
6. J. A. Duffie and W. A. Beckman, *Solar Engineering of Thermal Processes.* Wiley-Interscience, New York (1980).
7. G. C. Blytas and F. Daniels, Concentrated solutions of NaSCN in liquid ammonia, solubility, density, vapor pressure, viscosity, thermal conductance, heat of solution and heat capacity. *J. Am. Chem. Soc.* **84**, 1075 (1962).
8. S. L. Sargent and W. A. Beckman, Theoretical performance of an ammonia-sodium thiocyanate intermittant absorption refrigeration cycle. *Solar Energy* **12**, 137 (1968).
9. L. H. D. Fraser, Ammonium thiocyanate as an absorbent. *Refrigeration Engng* **24**, 20 (1932).
10. Rocket Research Co., Sulfuric acid-water chemical energy storage system. *Final Report for ERDA Contract* E(04-3)-1185 (1976).
11. R. H. Perry and C. H. Chilton (Editor), *Chemical Engineers Handbook*, 5th Edn. McGraw-Hill, New York (1973).
12. SOLMET Typical Meteorological Year, Tape Deck 9734, National Oceanic and Atmospheric Administration, Environmental Data Service, National Climatic Center, Asheville, North Carolina (1978).
13. M. O. McLinden, *Modeling and Simulation of Chemical Heat Pump Solar Heating Systems.* MS Thesis, University of Wisconsin-Madison (1980).